Advanced Reconfigurable Scaffolds Fabricated by 4D Printing for Treating Critical-size Bone Defects of Irregular Shapes

Chong Wang[1,†,*], Haibing Yue[2,3,†], Jia Liu[4,†], Qilong Zhao[5], Zhi He[1], Kai Li[6], Bingheng Lu[1], Wenhua Huang[7], Yen Wei[8], Yujin Tang[4,*], Min Wang[9,*]

[1]School of Mechanical Engineering, Dongguan University of Technology, Dongguan, Guangdong, P.R. China

[2]Department of Surgery, Li Ka Shing Faculty of Medicine, The University of Hong Kong, Hong Kong SAR, P.R. China

[3]Dr. Li Dak-Sum Research Centre, The University of Hong Kong - Karolinska Institutet Collaboration in Regenerative Medicine, The University of Hong Kong, Hong Kong SAR, P.R. China

[4]Department of Orthopaedics, Affiliated Hospital of Youjiang Medical University for Nationalities, Baise, Guangxi, P.R. China

[5]Institute of Biomedical & Health Engineering, Shenzhen Institutes of Advanced Technology (SIAT), Chinese Academy of Sciences (CAS), Shenzhen, P.R. China

[6]Department of Orthopedics, The Third Affiliated Hospital of Southern Medical University, Guangzhou, Guangdong, P.R. China

[7]National Key Discipline of Human Anatomy, School of Basic Medical Sciences, Southern Medical University, Guangzhou, Guangdong, P.R. China

[8]Department of Chemistry, Tsinghua University, Beijing, P.R. China

[9]Department of Mechanical Engineering, The University of Hong Kong, Pokfulam Road, Hong Kong SAR, P.R. China

Chong Wang[†], *Haibing Yue*[†] and *Jia Liu*[†] contributed equally.

Keywords: 4D printing; osteogenic peptide; black phosphorus; tricalcium phosphate; irregular bone defect

Corresponding authors: Dr. Wang C, Email: wangchong@dgut.edu.cn; Dr. Tang Y, Email: tangyujin1967@163.com; Prof. Wang M, Email: memwang@hku.hk

Abstract

While scaffold-based tissue engineering has been widely used to treat bone critical-size defects, challenges such as implantation of scaffolds in defects with irregular shapes and implantation of scaffolds through minimally invasive surgery remain in the tissue engineering field. Customized bioactive bone tissue engineering scaffolds with reconfigurable capability for both easy scaffold implantation and perfect shape fitting in irregularly shaped bone defects are therefore needed. Herein, applying 4D printing, photothermal-responsive shape memory bone tissue engineering scaffolds are constructed by incorporating black phosphorus (BP) nanosheets and osteogenic peptide into β-tricalcium phosphate/poly(lactic acid-*co*-trimethylene carbonate) (TCP/P(DLLA-TMC)) nanocomposite scaffolds. When near-infrared (NIR) irradiation is applied to customized scaffolds on-demand, scaffold temperature rapidly increases to 45 ^{o}C, enabling scaffold shape reconfiguration for easy scaffold implantation and precise fitting in irregular bone defects. Once the implantation is finished, scaffold temperature rapidly decreases to 37 ^{o}C and scaffolds display mechanical properties comparable to those of human cancellous bone. The improved osteogenesis in bone defect sites is then initiated through pulsed peptide release from scaffolds. Compact integration of reconfigurable scaffolds in rat cranial bone defects and improved new bone formation are demonstrated through micro-computed tomography and histochemical analyses. This study shows a facile method to clinically treat bone defects of irregular shapes.

1. Introduction

Traumatic injuries, infection, and tumor resection often result in critical-sized bone defects with an irregular shape, which are difficult to be healed by peripheral bone tissues themselves [1-3]. Injectable nonporous bone cements which have been developed for decades can perfectly fulfill the bone defects with an irregular shape, nevertheless, unexpected side-effects such as curing-related hyperthermia which is harmful to peripheral tissue may be involved [4]. Moreover, as bone cements are non-biodegradable, secondary surgery is needed to take out the cured bone cements when they are no longer needed.

Scaffold-based bone tissue engineering has emerged as a promising strategy to treat critical-sized bone defects. Among different fabrication techniques, cryogenic three-dimensional (3D) printing is advantageous in endowing scaffolds with designed hierarchically porous structure, sufficient mechanical strength and sustained delivery of osteoconductive and osteoinductive agents with a high initial loading level and a high biological activity, simultaneously [5], hence eliciting improved bone regeneration [6, 7]. However, considering the complexity of bone defects with irregular shapes, the direct fitting of 3D printed scaffolds with a customized pattern into irregular defects is highly difficult and additional surgical burdens may be caused to enable successful implantation [8]. Shape memory materials are good candidates to make reconfigurable scaffolds for treating irregular bone defects, as 3D printed shape memory scaffolds can be squeezed into the irregular bone defects at the transformation temperature (T_{trans}) [9-11]. Nevertheless, conventionally used shape memory matrix with a T_{trans} close to the body temperature cannot provide scaffolds with sufficient mechanical strength during bone regeneration process, whereas shape memory matrix with a too high T_{trans} would result in burn of the peripheral tissue and also the loss of the biological activity of the loaded biomolecules. Thus, shape memory matrix with

appropriate T_{trans} to both temporarily avoid burn of peripheral tissues/cells and possess sufficient mechanical strength at body temperature is urgently needed to produce reconfigurable scaffolds with required deformation/shape recovery capability and excellent mechanical support during bone regeneration. On the other hand, a suitable method to trigger fast shape recovery is also needed for the prompt and precise matching between the implanted customized scaffolds and the boundaries of irregular defects. In recent years, photothermal stimulation has emerged as a facile strategy to trigger the shape recovery of thermal-responsive materials. Single-layered black phosphorus (BP) has been proposed as one of the most promising nano-sized photothermal biomaterials due to the strong near-infrared (NIR) absorbance, high-photothermal-conversion efficiency, superior thermal conductivity and excellent cytocompatibility and degradability *in vivo*. In comparison, photothermal materials such as graphene, graphene oxide, MoS_2, etc., cannot degrade *in vivo* while polydopamine has a too high degradation rate (i.e., 40% weight loss within 24 h in PBS), although they all have excellent photothermal effects [1, 12-14]. Additionally, Poly(lactic acid-*co*-trimethylene carbonate) P(DLLA-TMC) has been used to fabricate thermo-responsive scaffolds with superior shape morphing feature [15], which makes it possible to construct 4D shape memory scaffold. Therefore, the combination of shape memory polymer matrix with photothermal agents allows the remote control of scaffold temperature when NIR irradiation is applied or withdrawn, hence bringing scaffolds with on-demand deformation/shape recovery capabilities, which are accompanied by the tuning of mechanical strength [16].

In this study, cryogenic four-dimensional (4D) printing which conceptually combines cryogenic 3D printing and the control of scaffold shape and mechanical strength over time was employed to produce reconfigurable bone tissue engineering scaffolds for treating bone defects with an irregular shape [17-19]. The scaffold was based on a composite design in which

biodegradable photothermal agents (i.e., BP nanosheets) and osteoinductive agents (i.e., osteogenic peptide which are functionally equivalent to bone morphogenetic protein-2 and highly potent to induce osteogenic differentiation *in vitro* and new bone formation *in vivo*), were incorporated into β-tricalcium phosphate/shape memory poly(lactic acid-*co*-trimethylene carbonate) (TCP/P(DLLA-TMC)) nanocomposite solutions to form printing inks, followed by printing of such inks in a cryogenic environment. The thermal-responsive shape memory TCP/P(DLLA-TMC) matrix endowed the scaffolds with great reconfiguration capability at 45 ºC for easy implantation in an irregular defect via a minimally invasive surgery and sufficient compressive strength at 37 ºC for long-term mechanical support; the biodegradable photothermal agents could induce shape recovery of the scaffold through NIR-induced hyperthermia during implantation and accelerate the release of osteogenic peptide upon pulsed NIR irradiation during the bone regeneration process. Finally, precise fitting of customized scaffolds in rat cranial defects with an irregular shape and improved bone regeneration were also obtained.

2. Results

2.1. Scaffold design

To treat irregular bone defects with a critical size, a reconfigurable scaffold with on-demand deformation/shape recovery capability, sufficient mechanical strength and improved bone-forming potent was designed (**Figure 1a**). The successful production of such a scaffold relies on the formulation of scaffold composition and the employment of appropriate fabrication technique, which ensured the integration of multiple functions within the same scaffold (**Figure 1b**). For easy implantation into a complex bone defect via a narrow path, the reconfigurable scaffold was firstly heated to 45 ºC, at which the modulus of the scaffold was significantly reduced (**Figure 1c**), and deformed into a temporary "slim" shape, followed by the cooling for shape fixation (**Figure 1d**).

During implantation, NIR irradiation was applied on the deformed scaffolds to guide shape recovery of scaffolds with the assistance of surgical instruments if necessary, enabling the precise matching of scaffolds into the defects with an irregular shape (**Figure 1e**). After the "matching", scaffolds with a permanent shape cooled down to the body temperature to show excellent mechanical strength that was similar to that of human cancellous bone and launch bone tissue regeneration. Eventually, improved bone regeneration was gradually achieved due to the controlled delivery of osteogenic peptide from the hierarchically porous bony environment.

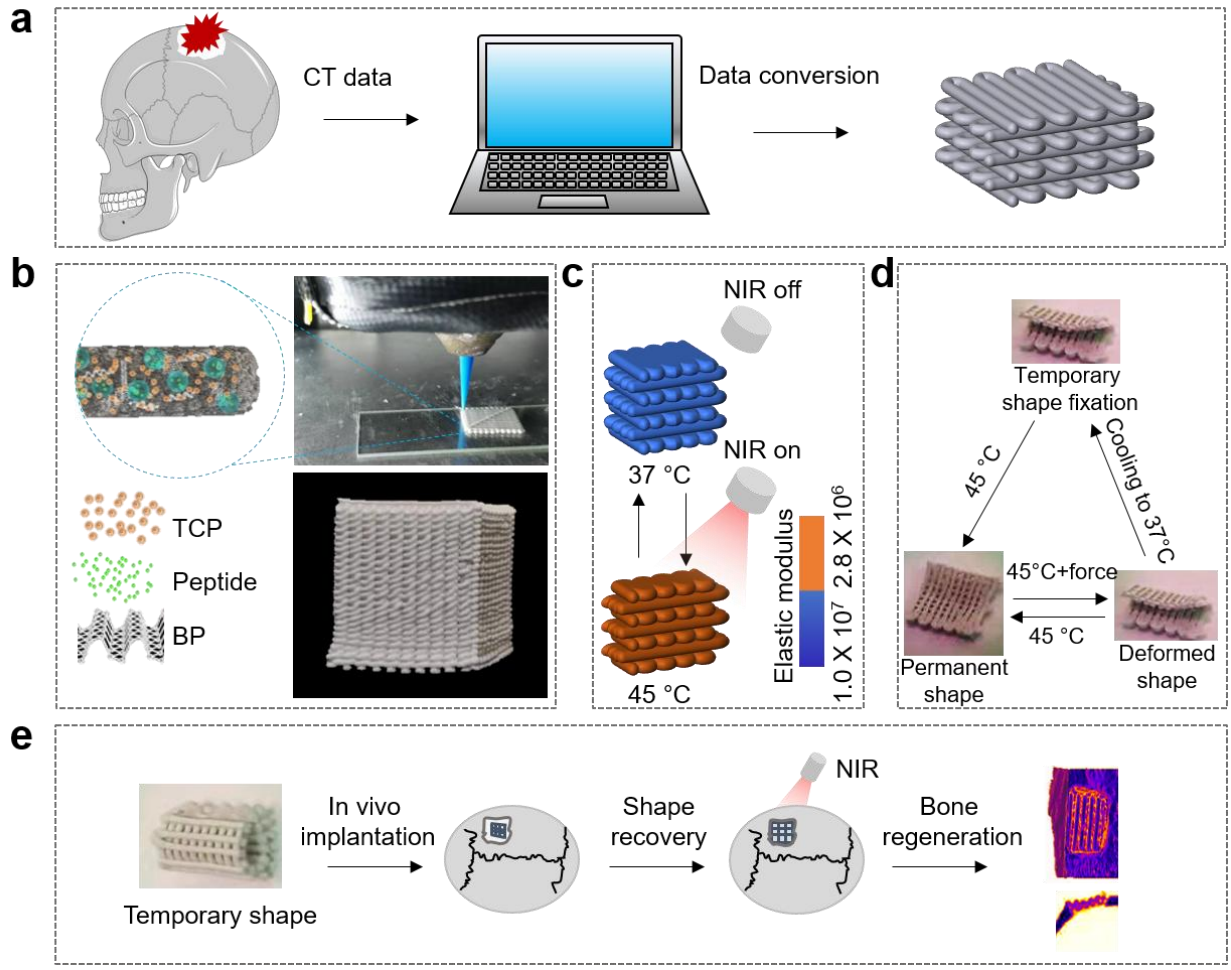

Figure 1. Schematic illustration of cryogenic 4D printing of BP and osteogenic peptide-loaded TCP/P(DLLA-TMC) shape memory scaffolds for easy scaffold implantation in an irregular bone

defect and *in vivo* bone regeneration: (a) 3D image data acquisition and 4D printing of scaffolds; (b) composition and printing process of peptide/BP/TCP/P(DLLA-TMC) scaffold; (c) NIR irradiation increased the scaffold temperature and decreased the scaffold modulus; (d) Increased scaffold temperature enabled the scaffold deformation/shape recovery; (e) deformed scaffold can be easily implanted into irregular bone defect and get recovered to launch customized bone regeneration.

2.2. Scaffold characterization

The TEM micrograph shows the structure of BP nanosheets (**Figure S1**). The reconfigurable scaffolds ("BTPS") were structurally identical to the CAD models, showing a well-controlled macroporous 3D pattern (**Figure 2a** and **b**). Inter-connective square holes with a side length of 360 ± 40 μm were observed from the top-view and cross-section (**Figure 2c** and **d**). The scaffolds had a rough strut surface on which micropores with a diameter of 5-20 μm can be observed (**Figure 2e**), showing a hierarchically porous structure. A number of TCP particles with a diameter of less than 200 nm were observed on the surface of the P(DLLA-TMC) matrix, showing a uniform TCP distribution (**Figure 2f**).

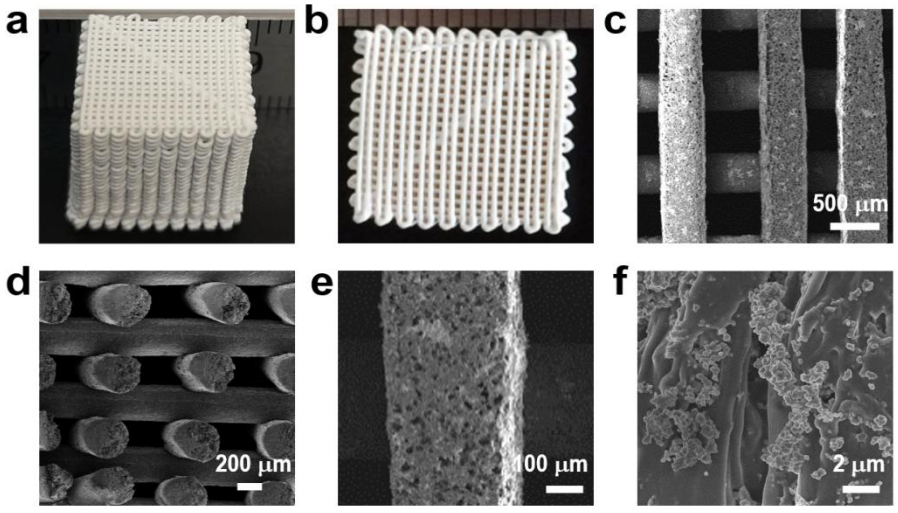

Figure 2. Morphology of BP/peptide/TCP/P(DLLA-TMC) scaffolds: (a-b) digital images of scaffolds with different visual angles; (c-d) SEM micrographs of scaffold surface and cross-section; (e) magnified SEM micrograph shows the microporous structure of scaffold strut; (f) magnified SEM micrograph shows the morphology of incorporated TCP particles.

The mechanical properties of reconfigurable scaffolds and controls were investigated through compression testing. All scaffolds immersed in PBS at 20 ^{o}C had compressive strengths and elastic moduli of 2.2 ± 0.2 to 2.4 ±0.2 MPa and 22.1 ± 3.1 to 22.0 ± 2.1 MPa, respectively, whereas scaffolds at 37 ^{o}C had compressive strengths and elastic moduli of 1.5 ± 0.2 MPa and 10.2 ± 1.4 MPa, respectively, which were still comparable to that of human cancellous bone under the physiological condition, suggesting that our scaffolds were mechanically suitable to repair cancellous bone tissue (**Figure 3a** and **b**) [20]. In comparison, when the temperature increased to 45 ^{o}C which is close to the glass transition temperature of shape memory matrix, scaffolds became soft (i.e., compressive strengths and elastic modulus decreased to 0.4 ± 0.05 MPa and 2.8 ± 0.2 MPa, respectively) and could be greatly deformed into a "slim" state which was favorable for minimally invasive implantation in irregular defects. It is also found that the mechanical properties of composite scaffold can be restored to the level before deformation. After scaffold deformation, the temporary shape could be fixed by cooling down to room temperature. When the deformed scaffolds (either in stretched, folded or compressed state) were subjected to NIR irradiation and the scaffold temperature achieved 45 ^{o}C, shape recovery to the permanent structure occurred (**Figure 3c**). As high as 95% shape recovery within 30 s were realized, no matter which type of deformation was applied beforehand (**Figure 3d**).

Apart from heating scaffolds to a certain temperature in an oven or a warm water bath, the NIR irradiation on BTS and BPTS scaffolds could also increase the scaffold temperature due to

the excellent photothermal conversion efficiency of incorporated BP nanosheets, hence providing an on-demand approach to guide shape recovery remotely. When the power density increased from 0.5 to 2.0 W cm^{-2}, the scaffold temperature increased from 37 to 55 ^{o}C in 10 min under wet condition (**Figure 4a**). The temperature of BP loaded scaffolds increased rapidly in a short time upon NIR irradiation, and then maintained a stable temperature as irradiation time increasing due to the balance between heat production and dissipation. In comparison, scaffolds without BP incorporation had no photothermal effect and maintained at room temperature under NIR irradiation (**Figure 4b**). The red area in **Figure 4c** represented the high-temperature area of scaffolds. The observed temperature distribution could be attributed to the varied heat generation/dissipation balance in different regions of the scaffold samples. As more heat can be dissipated from the peripheral area than the central area, lowered temperature can be obtained for the peripheral area. In the current study, the highest temperature shown on the thermal image (normally the central part has the highest temperature) was used to represent the temperature of the whole scaffold sample [13]. The shape recovery of the deformed BTS and BPTS scaffolds with a recovery ratio of 90% could be triggered by 60 s of NIR irradiation at a power density of 2.0 W cm^{-2} (**Figure 4d** and **e**), The deformation, shape maintenance and NIR-triggered shape recovery of reconfigurable scaffolds are also shown (**Figure 4f, Movie S1**). **Figure 4g** shows the implantation of three types of BTPS scaffolds (i.e., “five-point star”-, “T”- and “ladder” shape) into model defects with matched shapes through narrow implantation channels. With the assistance of surgical instruments (if necessary) and NIR irradiation, excellent deformation, smooth implantation, rapid shape recovery and precise matching between the irregular defects and customized scaffolds were achieved. Moreover, regular macropores in the implanted scaffolds were retained which were identical to that before the scaffold deformation.

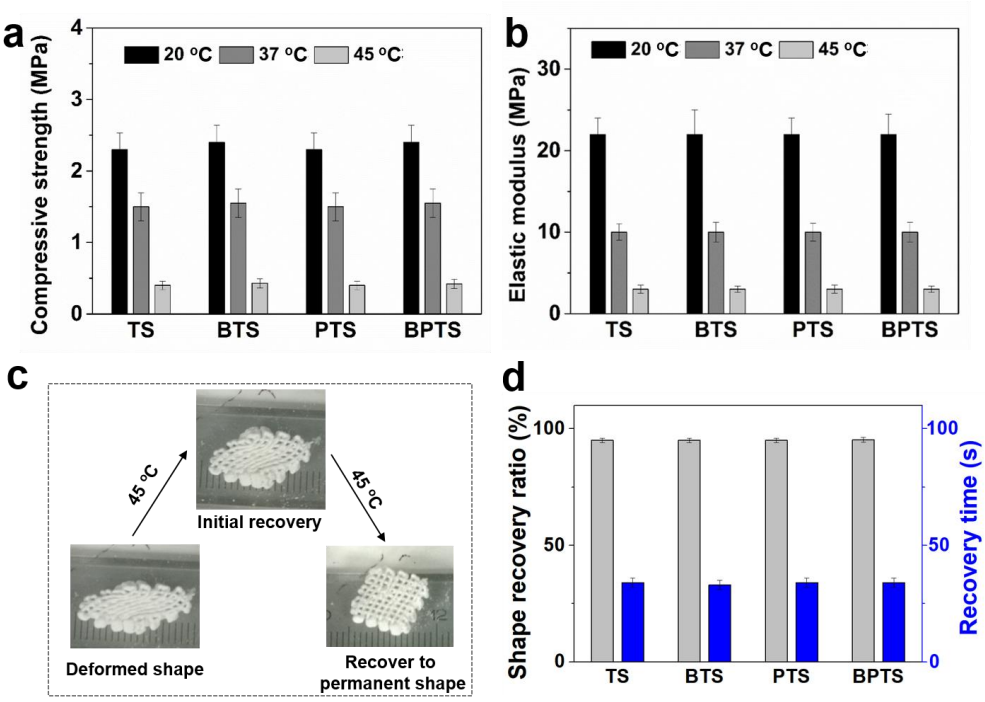

Figure 3. Mechanical properties and shape memory effect of BP/peptide/TCP/P(DLLA-TMC) scaffolds: (a) compressive strength; (b) Young's modulus; (c) shape recovery of scaffolds in the water at 45 ºC; shape recovery ratio and recovery time in the water at 45 ºC.

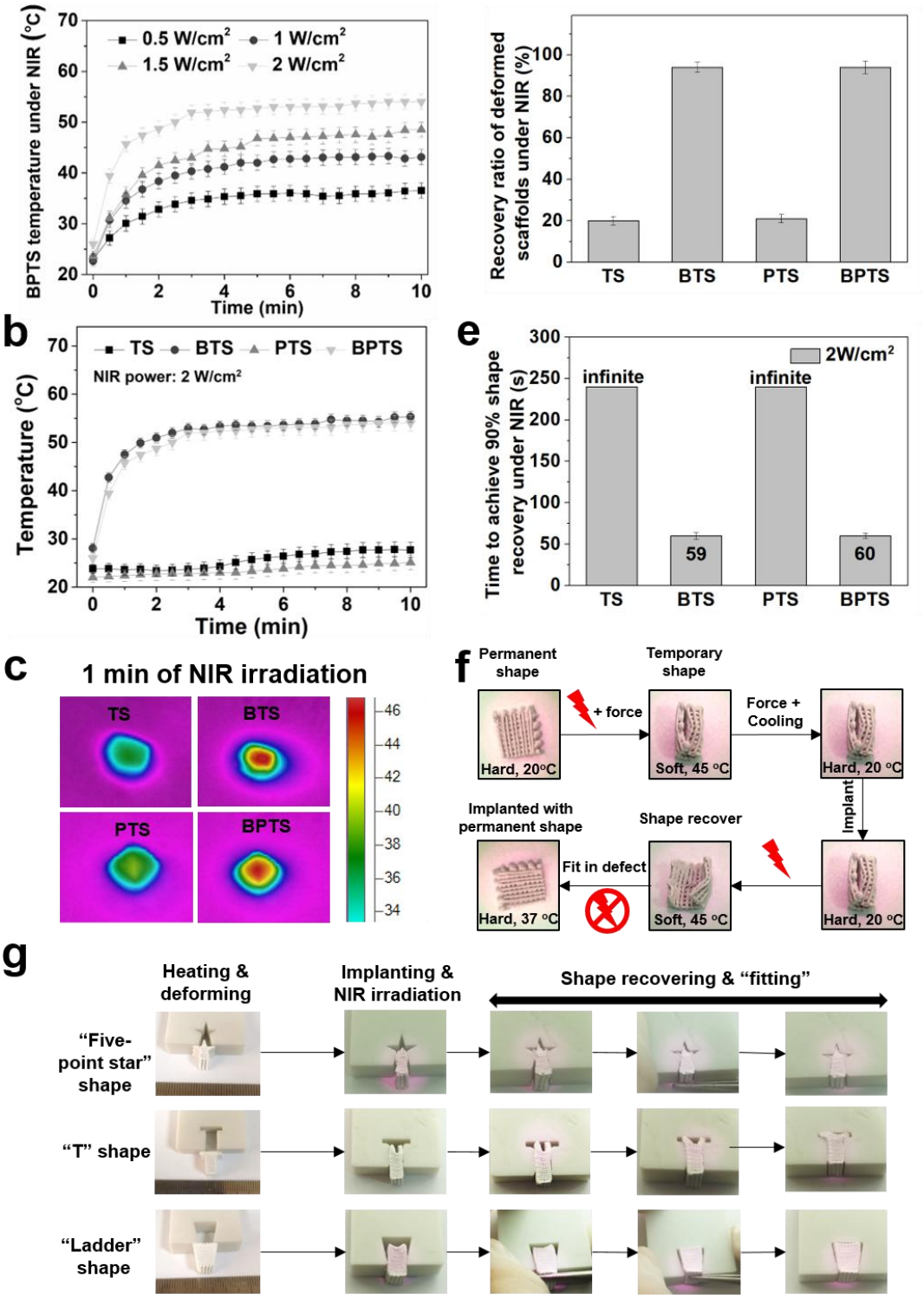

Figure 4. Photothermal effect of scaffolds: (a) temperature increase of BPTS scaffolds under different NIR power density; (b) temperature increase of different scaffolds under the same NIR; (c) temperature distribution on different scaffolds under NIR; (d) recovery ratio of scaffolds under

NIR; (e) recovery time of scaffolds under NIR; (f) shape memory cycle of BPTS scaffolds, from original shape to deformed shape and further to recovered shape.

2.3. *In vitro* osteogenic peptide release and scaffold degradation

Sustained release of the osteogenic peptide from reconfigurable scaffolds is important to induce bone regeneration. In this study, with the assistance of NIR-irradiation, on-demand peptide release can be obtained (**Figure 5a**). When no NIR irradiation was applied, an initial peptide release of 18% in 24 h followed by a slow but steady release up to 53% within 24 days was obtained for PTS scaffolds (**Figure 5b** and **c**). A slightly lowered peptide release was obtained for BPTS scaffolds owing to the enhanced adsorption of released peptide on to the BPTS scaffolds which had a slightly larger surface area due to the presence of BP nanosheets. In comparison, the peptide release from BPTS was found to be greatly accelerated by periodical NIR irradiation (i.e., applied every other day), in which a 1.5-fold peptide release was obtained after irradiation, showing a pulsed peptide release profile. *In vitro* degradation behaviour of different scaffolds in an 8-week test period is shown in **Figure S2**. As P(DLLA-TMC) matrix has a relatively low degradation rate and only a small amount of osteogenic peptide and BP nanosheets were incorporated in scaffolds, no significant difference of the weight loss can be found in different scaffolds, and only 7% weight loss can be obtained after 8 weeks of incubation.

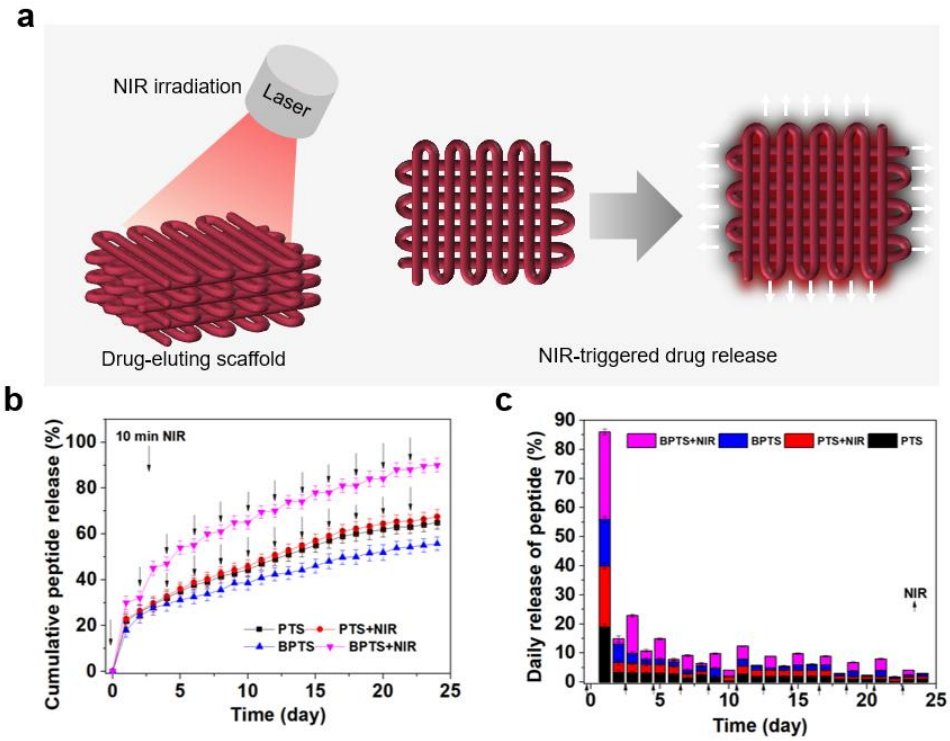

Figure 5. *In vitro* release behavior of peptide from scaffolds: (a) schematic illustration of NIR-induced osteogenic peptide release; (b) cumulative release of peptide from different scaffolds with or without pulsed NIR irradiation; (c) daily release percentage of peptide from different scaffolds with or without pulsed NIR irradiation.

2.4. *In vitro* rBMSC osteogenic differentiation and *in vivo* bone regeneration

Figure 6a shows the viability of rBMSCs on scaffolds after a 3-day culture. Nearly all rBMSCs on all scaffolds were alive (color in green), suggesting our multifunctional scaffolds were biocompatible. The effect of pulsed NIR irradiation on the viability of rBMSCs seeded on BTS and BPTS scaffolds is shown in **Figure S3**. When the culture temperature increased from 37 to 40 ^{o}C, no more cell death was detected. Meanwhile, rBMSCs located at the peripheral area and the central area showed similar cell viability. Compared to BTS and TS scaffolds, rBMSCs on BPTS and PTS scaffolds showed significantly improved proliferation ($p < 0.05$), while BTS induced

slightly higher rBMSC proliferation than TS scaffolds (**Figure 6b**). As the temperature of the reconfigurable scaffolds could increase to 47 ºC upon NIR irradiation, whether peptide could maintain its stability and biological activity at such temperature is concerned. The osteogenic differentiation of rBMSCs induced by peptide-containing medium maintained at 37, 40, 45 and 47 ºC for 10 to 30 min, respectively, was then compared. As shown in **Figure 6c**, after 7-day culture, rBMSCs cultured in medium supplemented with osteogenic peptide treated below 45 ºC had similar level of alkaline phosphatase (ALP) activity (osteogenic peptide at 40 ºC showed the highest osteogenic differentiation potent), whereas peptide treated at 47 ºC showed slightly lowered ALP activity, suggesting the osteogenic peptide could mostly maintain its stability below 47 ºC, whereas longer incubation time at 47 ºC would reduce the biological activity of peptide. The effect of scaffolds with the assistance of pulsed NIR irradiation (targeting temperature of 40 ºC) on osteogenic differentiation of rBMSCs was then investigated by measuring ALP activity of rBMSCs on scaffolds at day 7 and 14. Comparing to TS scaffolds, BTS scaffolds slightly up-regulated the ALP activity while PTS scaffolds significantly up-regulated the ALP activity (**Figure 6d**). In comparison, BPTS group showed the highest level of ALP activity, suggesting that the pulsed peptide release with an accelerated release rate could improve the rBMSC osteogenic differentiation. It is found that the ALP activity obtained on day 7 was higher than that on day 14 for all groups. As ALP is an early marker during the osteogenic differentiation of rBMSCs, more ALP can be expressed after 7 days of culture. Meanwhile, the rBMSCs cultued for 14 days are more senescent than rBMSCs cultured only for 7 days; thus less ALP is expressed by rBMSCs after 14 days of culture. Other studies also confirmed this phenomenon [+1]. The same trend was also verified by the ALP staining results in which the extracts of PTS and BPTS scaffolds induced significantly higher amount of ALP expression than that of TS and BTS scaffolds after 7-day

culture (**Figure 6e**).

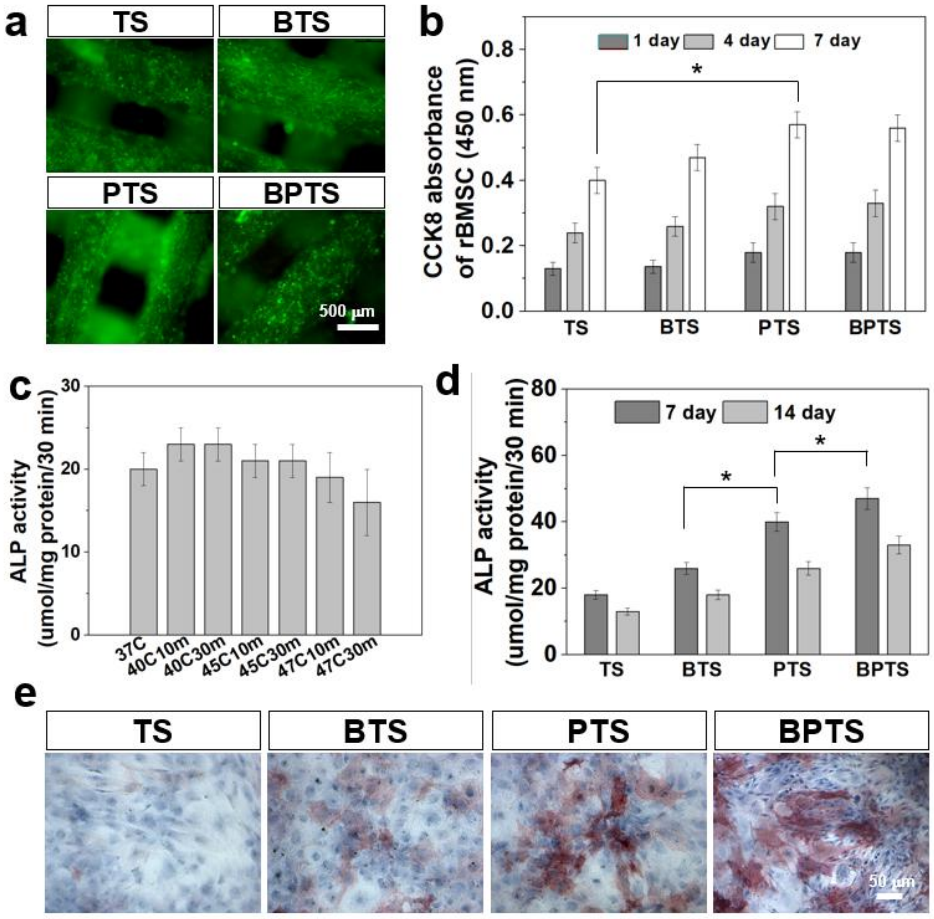

Figure 6. *In vitro* biological performance of scaffolds: (a) live and dead staining of rBMSCs on scaffolds after 3-day culture; (b) proliferation of rBMSCs on scaffolds with increasing culture time; (c) ALP activity of rBMSCs when cultured with peptide treated at different conditions; (d) ALP activity of rBMSCs cultured on different scaffolds; (e) ALP staining of rBMSCs culture with extracts of scaffolds for 7 days.

The *in vivo* bone regeneration was studied by monitoring the *in vivo* bone formation for 3 months. Irregular cranial defects with an approximate dimension of 3 mm × 5 mm × 1 mm were created on cranial bone tissue of rats to establish animal model and scaffolds with a slightly enlarged size (3.3 mm × 5.5 mm × 1 mm) were compressed and implanted via minimally invasive

surgery, assisted with NIR irradiation (**Figure 7a**, n=4 for each group). The NIR irradiation with a targeting temperature of 40 ºC was applied on each implanted scaffold for 10 min every other day, up to 30 days. It can be seen from μ-CT images that, 3 months after surgery, very limited new bone formation was observed in the control group, whereas discernable new bone formation was observed in TS scaffolds (the μ-CT images picked up not only new bone but also undegraded scaffold materials), however, unfilled cavities can still be found. In comparison, BTS scaffolds enhanced the new bone formation, while PTS and BPTS scaffolds significantly up-regulated the new bone formation, in which obvious new bone tissue was observed on scaffold struts and most pores in scaffolds were filled by new bone tissue (**Figure 7b**). It is worth noting that unfilled cavities still can be found at the host bone/scaffold boundary for TS, PTS groups, indicating an incompact union between scaffolds and peripheral bone, which could be attributed to the insufficient scaffold shape recovery, as no BP was incorporated in TS and PTS scaffolds. In comparison, the compact union between BP-containing scaffolds (i.e., BTS and BPTS) and the irregular boundary can be observed due to the shape recovery-induced shape fitting at 45 ºC and locking at 37 ºC. **Figure 7c** shows the bone volume/total volume (BV/TV) ratio of each group containing un-degraded scaffolds. 64.6 ± 2.6, 70.3 ± 9.9 and 78.2 ± 10.7% new bone formation was achieved for BTS, PTS and BPTS scaffolds after 3 months, respectively, whereas only 13.7 ± 6.9 and 35.1 ± 16.2% new bone volume were induced by negative control and TS scaffolds, respectively. **Figure 7d** shows the bone mineral density (BMD) of defected areas implanted with different types of scaffolds. Likewise, the BMD value of BTS, PTS and BPTS groups was significantly higher than Control and TS groups (380 ± 53, 409 ± 49 and 470 ± 83 vs. 71 ± 23 and 200 ± 65 mg/cm^3, $p < 0.05$).

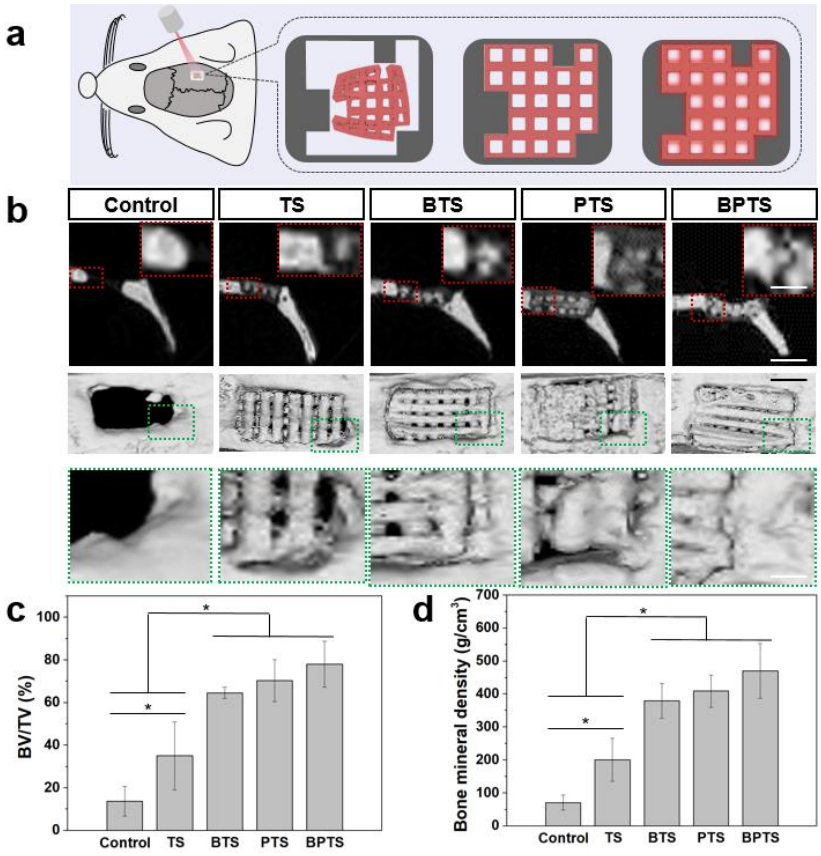

Figure 7. *In vivo* regeneration of rat cranial defects: (a) schematic illustration of *in vivo* scaffold implantation in irregular rat cranial defects with the assistance of NIR irradiation; (b) typical μ-CT images of regenerated cranial bone defects; (c) bone volume/total volume (BV/TV) ratio of regenerated tissue; (d) bone mineral density of regenerated bone tissue.

The H&E staining and Masson's trichrome staining were subsequently conducted to examine the tissues regenerated in each group (**Figure 8**). Scaffolds (labeled with 'S') could be observed in all groups except the negative control group. Similar to the results obtained from micro-CT data, the histological examinations revealed variable amounts of new bone formation in different groups. Tissues regenerated in negative control groups had the lowest thickness and only very limited new bone formation was observed at the peripheral part of the defects, whereas a large amount of fibrous tissues were observed at the central part of defects. In comparison, significantly more

mineralized centers (labeled with red stars) were found in TS group, indicating TS scaffolds had excellent osteoconductivity which supported the bone ingrowth. Towards BTS, PTS and BPTS groups, much more new bone and bone trabecula structure (labeled with red stars) were observed (i.e., dark blue area in the Masson's trichrome staining images), which fulfilled the pores of the scaffolds. Moreover, crawling of new bone tissue on both sides of scaffolds was also observed in these groups, suggesting our reconfigurable scaffolds were favorable platforms for inducing bone regeneration.

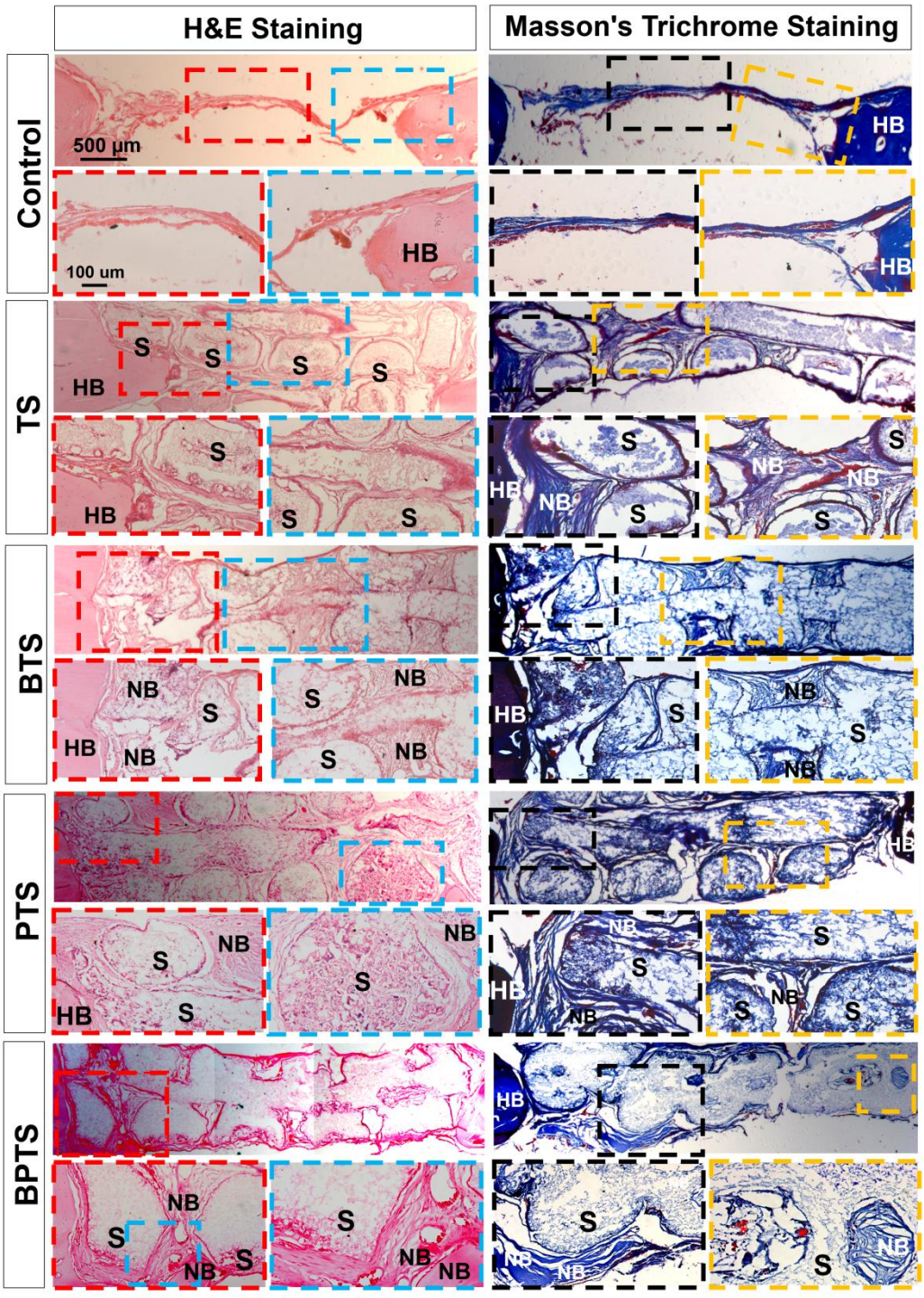

Figure 8. Histological analysis of regenerated tissues in the rat cranial defects 3 months after the implantation of different scaffolds through H&E staining and Masson's trichrome staining. Micrographs with a low magnification show the sectioned slice of entire cranial defect region.

H&E micrographs with a high magnification show the representative images of scaffolds embedded in regenerated tissues in different regions. Masson's trichrome staining micrographs with a high magnification show the representative images of the edge and central area of the defects. Notes: "S" represents scaffold; "HB" represents host bone; "NB" indicates the new bone and osteoid.

3. Discussion

The treatment of bone defects is of great importance to maintain the patient's body integrity and is favorable for subsequent motor function rehabilitation [21, 22]. So far, scaffold-based tissue engineering has been increasingly used to treat critical-sized bone defects due to a number of advantages, however, tissue regeneration in bone defects with an irregular shape cannot be easily solved by scaffold-based tissue engineering, as several critical requirements including easy scaffold implantation and prompt shape matching, on-demand adjustment of mechanical strength of scaffolds and improve bone formation via controlled delivery of osteogenic agents are difficult to be fulfilled at the same time. In this study, a cryogenic 4D printing strategy based on cryogenic 3D printing and the control of scaffold shape and mechanical strength over time was adopted to produce a reconfigurable bone tissue engineering scaffold. The advantages of using cryogenic 4D printing to fabricate such scaffolds include: (1) customized shape to match irregular defects; (2) hierarchically porous structure to enable both improved cell penetration and attachment; (3) on-demand shape deformation and recovery with tunable mechanical strength and (4) *in situ* delivery and controlled release of osteogenic peptide for improved bone regeneration. With the above advantages, minimally invasive scaffold implantation with a quick shape adaptation, on-demand tuning of mechanical strength of scaffolds and controlled release of osteogenic peptide can be simultaneously achieved. Since composite emulsions are viscous fluids at room temperature, the

3D printing of such inks at room temperature has much lower printing accuracy due to the collapse of the printed struts. Hence cryogenic environment can be used to improve the 3D printing accuracy as the as-extruded emulsion inks can be rapidly frozen into stable pattern under a cryogenic environment. For instance, the dimension of cryogenic 4D printed scaffolds is identical to that of the CAD file. Compared to scaffolds produced through casting techniques, cryogenic 4D printed scaffolds are advantageous in endowing scaffolds with hierarchically porous structures (i.e., interconnected macropores in 3D patterns and micropores on strut surface). This not only up-regulates the cell migration into the inner part of the scaffolds but also improves the initial cell attachment and spreading. Towards the scaffold implantation, as shape memory P(DLLA-TMC) with a T_{trans} of 45 ^{o}C was used as the scaffold matrix, dramatic scaffold deformation from its customized permanent shape to a deformed temporary shape at 45 ^{o}C could be obtained, which is favorable for the scaffold transport to the irregular defect [23]. As shown in **Figure.4g** and **Figure.7b,** the on-demand photothermal stimulation triggered the shape recovery of scaffolds, enabling the precise "matching" of scaffolds in the irregular defects *in vitro* and *in vivo* [24]. So far, photothermal polymers such as polydopamine (PDA) nanoparticles and several types of 2D photothermal materials including graphene, MoS_2, WSe_2, h-BN and BP nanosheets have been used for biomedical applications. Although 2D graphene, MoS_2 and WSe_2 have excellent photothermal conversion efficiency, they are not biodegradable and this severely restricts their applications *in vivo*. In comparison, BP nanosheets and PDA exhibit not only excellent photothermal conversion efficiency (36% vs. 40%) and capability for photodynamics treatment but also desirable biocompatibility, biodegradability and drug/biomolecule delivery capability. In this study, BP nanosheets are more advantageous than PDA nanoparticles as BP could be uniformly embedded in the P(DLLA-TMC) matrix to gain elongated photothermal capability whereas PDA

nanoparticles could be only placed on the surface of micropores and the photothermal effect may decay rapidly due to higher degradation rate of PDA (i.e., as high as 40% weight loss can be obtained for PDA nanoparticles within 24 h). Besides, BP nanosheets have higher surface area-to-volume ratio than PDA nanoparticles, thus BP nanosheets have stronger capability to physically or non-specifically adsorb molecules. After the "matching", NIR irradiation was withdrawn and scaffold was quickly cooled down to 37 ^{o}C, exhibiting a compressive strength comparable to human cancellous bone. Such excellent compressive strength making it feasible to provide favorable long-term mechanical support for targeting bone tissue (i.e., cancellous bone) during the repair/regeneration process, hence up-regulating new bone formation. In comparison, some biomaterials such as hydrogel- or electrospun polymer fiber-based scaffolds which have insufficient mechanical strength (especially compressive strength) cannot be used to repair/regenerate bone tissues with some load-bearing capabilities.

Towards the tissue regeneration in irregular bone defects, the cryogenic 4D printed reconfigurable scaffolds with a hierarchically porous structure were favorable for rBMSC anchorage, spreading and osteogenic differentiation. The *in situ* delivery of osteogenic peptide in the scaffolds greatly improves the rBMSC osteogenic differentiation *in vitro* and new bone formation *in vivo* [25, 26]. Among various osteogenic agents including growth factors, peptide and inorganic trace elements (e.g., magnesium, manganese, etc.), bone morphogenetic protein-2 (BMP-2) is well recognized as the most potent agent to induce osteogenesis *in vitro* and *in vivo*. Thus, in this study, we select osteogenic peptide which is functionally equivalent to BMP-2 (i.e., osteogenic peptide and BMP-2 bind the same receptor to activate the signaling pathway of osteogenesis) to improve bone tissue regeneration. However, like BMP-2, the osteogenic peptide is also thermal-sensitive, hence whether the biological activity of the osteogenic peptide could be

maintained after the photothermal treatment is concerned. Our results showed that the osteogenic peptide heated to 45 ºC for 10 min induced similar level of ALP activity of rBMSCs, comparing to that at 37 ºC, suggesting the osteogenic peptide could survive the short-term photothermal stimulation and induce rBMSC osteogenic differentiation afterward. Different from other studies that adsorbed molecules onto the surface of scaffolds to realize a short-term release, as high as 2.7 mg of peptide was uniformly distributed in 1 g of hierarchically porous scaffolds. When no NIR irradiation was applied, a prolonged peptide release consisting of an initial burst release and a slower but sustained release was achieved. The initial peptide release could be attributed to the dissolution of peptide from micropores located on or near the scaffold surface into the test liquid, while the sustained peptide release could be attributed to (1) the diffusion of peptide from the micropores located at the inner layer of the struts to the test liquid and (2) the matrix degradation induced-accelerated peptide diffusion [27]. It is worth noting that the periodical NIR irradiation on BPTS scaffolds could obviously accelerate the peptide release in a pulsed manner, as the NIR irradiation could quickly increase the temperature of scaffolds from 37 to 40 ºC and turn the scaffolds from a hard state to a rubbery state, resulting in faster peptide diffusion from the inner layer of struts to the test liquid [28, 29]. Compared to TS scaffolds, PTS scaffolds with sustained delivery of osteogenic peptide not only supported the rBMSC proliferation but also up-regulated the rBSMC osteogenic differentiation. The further improved rBMSC osteogenic differentiation *in vitro* by BPTS scaffolds could be attributed to the accelerated peptide release induced by pulsed photothermal stimulation. However, whether tissue barriers will affect the NIR irradiation induced-photothermal effect of scaffolds implanted *in vivo* is still concerned. Tong *et al.* fabricated BP/PLGA membranes with a BP content of 0.2 wt% [30]. They found that even a thick pork tissue pieces (e.g., 7 mm) was used as a tissue barrier, a 5 ºC temperature increase can still be obtained

when NIR irradiation with a power density of 1 W/cm^2 was applied. In our study, as the BP content in the composite scaffolds is set as 0.15 wt% and the power density of NIR light is set as 2 W/cm^2, sufficient photothermal conversion can be still obtained to achieve a target temperature of 40 ^{o}C for our scaffolds implanted in rat cranial defects. Towards implantation of BP containing composite scaffolds in human bone defects which have a larger barrier thickness, higher BP content and NIR light density can be employed to resolve the insufficient temperature increase. In addition, BP nanosheets that are directly exposed to the aqueous environment could gradually degrade into phosphates, hence providing concentrated phosphates to participate in cell mineralization [30, 31]. The *in vivo* study also confirmed this trend as BTS scaffolds induced higher volume of new bone formation than TS scaffolds while BPTS groups showed the highest bone regeneration volume and BMD value due to the synergistic effect of pulsed release of osteogenic peptide and the presence of BP and TCP. The substantial new bone formation within and at the peripheral area of the scaffolds suggests bioactive scaffolds with capabilities of on-demand reconfiguration and controlled peptide release are excellent candidates for treating bone defect with an irregular shape.

4. Conclusions

In this investigation, advanced bone tissue engineering scaffolds with on-demand deformation/shape recovery capability, adjustable mechanical strength and excellent bone-forming ability were successfully produced through cryogenic 4D printing. The matrix polymer provided shape recovery ability for scaffolds and BP nanosheets and osteogenic peptide could be incorporated in hierarchically porous nanocomposite scaffolds. The thermal-responsive scaffold matrix for shape changes and the on-demand NIR irradiation enabled easy implantation through a narrow channel of scaffolds in bone defects of irregular shapes and also maintenance of high compressive strength of scaffolds during bone regeneration. The *in situ* incorporated osteogenic

peptide could be released from the advanced scaffolds in a controlled manner, thus improving rBMSC osteogenic differentiation *in vitro* and enhancing the bone regeneration in cranial defects of rats *in vivo*, while the BP nanosheets exhibited a supportive effect on *in vitro* rBMSC osteogenic differentiation and *in vivo* bone regeneration. This study has demonstrated a facile method to treat irregular bone defects and this strategy can be readily extended to repairing other hard and soft tissue defects of irregular shapes.

5. Experimental Section

Materials: Poly(D,L-lactic-co-trimethylene carbonate) P(DLLA-TMC) with an inherent viscosity of 0.8 dL/g, a DLLA/TMC ratio of 95:5 and a glass transition temperature (Tg) of 45 ºC was provided by Jinan Daigang Biotechnology Ltd, Shandong, China. β-tricalcium phosphates (β-TCP) with an average diameter of < 10 μm were supplied by Shanghai Bio-lu Biomaterials Co., Ltd, China. Black phosphorus (BP) crystal was provided by Nanjing Muke nanotechnology, Ltd, China. The osteogenic peptide with a sequence of KIPKA SSVPT ELSAI STLYL SGGC and a purity of 98.12% was provided by Shanghai Ziyu Biotechnology Co., Ltd. Collagen type I (from rat tail) was supplied by Corning, Inc., USA. DI water for all experiments was obtained using a DI water producer (Model D12681, Barnstead International, USA). Tween 20, phosphate-buffered saline (PBS) tablets were Sigma-Aldrich products (USA). dichloromethane (DCM) was supplied by Uni Chem Co., Korea.

Formation of BP/peptide/TCP/P(DLLA-TMC) water-in-oil composite emulsion inks: BP nanosheets were prepared following the protocol adopted in our previous investigation[5]. 9 mg of BP nanosheets was added into 10 mL of P(DLLA-TMC)/DCM solution (24%, w/v) to obtain BP/P(DLLA-TMC) solution with uniform BP distribution. 0.9 mL of DI water was then blended with 10 mL of as-prepared BP/P(DLLA-TMC)/DCM suspension, 50 μL of Tween 20 and 3.6 g of

β-TCP nanoparticles. After 5 min ultra-sonication, water-in-oil emulsion inks with uniform β-TCP distribution were successfully formed, followed by the addition of 200 μL of collagen I solution (9.5 mg/mL, as a stabilizer), 2.3 μL of NaOH (1 N), 10 mg of peptide, forming printing inks for producing multifunctional scaffolds. Collagen I was incorporated in the ink to improve the biocompatibility of scaffolds and enhance the cell affinity on scaffold surface. The as-printed BP/peptide/TCP/P(DLLA-TMC) scaffolds were designated as "BPTS". Other control inks and printed scaffolds such as peptide/TCP/P(DLLA-TMC), BP/TCP/P(DLLA-TMC) and TCP/P(DLLA-TMC) scaffolds were designated as "PTS", "BTS" and "TS", respectively.

Fabrication of BPTS scaffolds through cryogenic 4D printing: Before cryogenic 4D printing, BPTS inks were transferred into a 20 mL syringe connected with a plastic V-shape nozzle (inner diameter: 0.4 mm). After loading the syringe into the locator of a printing machine, a pre-designed CAD model was opened in the printing software. According to the CAD model (each scaffold had a 45-layer structure and each layer consisted of 20 paralleled rods with a length of 15 mm and a diameter of 0.5 mm; rods in adjacent layers had a cross angle of 90 °), BPTS scaffolds were constructed with a printing speed of 8 mm/s and a layer thickness of 0.3 mm at an environmental temperature of -10 °C and a programmed screw with a feeding rate of 0.008 mm/s was used to pump the piston of the syringe to extrude inks. A fan was placed on the stage to provide continuous flow to remove DCM. After the model construction, the scaffold was cryo-dried for 1 h to remove the residual DCM.

Scaffold characterization: The structure and morphology of BP nanosheets and β-TCP were studied using TEM and SEM. respectively. The macro- and microscopic morphology of 3D printed scaffolds were observed using digital camera and SEM (Leo 1530 Gemini, Zeiss, Oberkochen, Germany), in which scaffold samples were freeze-dried for 24 h, followed by the coating of a thin

layer of gold. Compression tests of scaffolds with a strain rate of 2 mm/min were conducted at 20, 37 and 45 ºC under wet conditions, respectively. The dimension of the tested samples was 5 mm × 5 mm × 5 mm. 5 samples were tested for each type of scaffolds. The deformability and shape memory effect of scaffolds was studied by measuring shape recovery rate and shape recovery speed.

In vitro photothermal performance: The *in vitro* photothermal performance of scaffolds was investigated by irradiating scaffold samples in an individual well of a 48-well culture plate (Corning, USA) at a power density of 0.5 to 2.0 $W \cdot cm^{-2}$. NIR laser was generated by an 808 nm high power multimode pump laser. The temperature value and the corresponding thermal images of the irradiated sites were recorded on an infrared thermal imaging instrument (Fluke Ti450, USA). The photothermal performance of different scaffolds and photo-stability of scaffolds were also measured at a power density of 2 $W \cdot cm^{-2}$. The effect of NIR irradiation on the shape recovery of BP containing scaffolds was also investigated. The process of scaffold deformation, implantation and NIR-induced shape recovery of BTPS scaffolds in three types of irregular defects was recorded using a digital camera.

In vitro release of osteogenic peptide: The peptide grafted with FITC was used as a model peptide to conduct the *in vitro* release tests. To investigate *in vitro* releases of the osteogenic peptide, pre-weighed scaffold samples were put in test tubes filled with PBS solutions supplemented with additives (0.02% sodium azide, 0.1% BSA, 0.05% EDTA, 0.1% heparin for peptide release tests). The test tubes were put in a shaking water bath at 37 ºC. At pre-determined time intervals, the test liquid was taken out and the concentration of peptide was measured using a fluorescence microplate reader. The effect of NIR irradiation on the release behavior of peptide from BPTS scaffolds was also studied. Typically, NIR irradiation was applied on scaffolds for 10 min every

other day, with a target temperature of 40 ºC.

In vitro osteogenic differentiation of rBMSCs: rBMSCs were cultured with Dulbecco's modified Eagle's medium/F-12, (DMEM/F-12, Gibco, USA) which was supplemented with 10% fetal bovine serum (Biowest, France), 100 U/ml penicillin-streptomycin and 2 mM L-glutamine (Invitrogen, USA) and maintained in a humidified incubator at 37 ºC with 74.1% N_2, 19.95% O_2 and 5% CO_2. Towards the cell seeding on scaffolds, scaffolds samples with a 4 layer structure (5 mm × 5 mm × 1.2 mm) was put in wells of a 24-well plate, followed by addition of 50 μL of culture medium in each well (to humidify the scaffold samples). Afterward, 100 μL of hBMSCs with a density of 1×10^6 were dripped on the struts of scaffolds. As scaffolds had a grid pattern, not all cells can precipitate on the struts and some of the cells will go down to the bottom of the well. After 8 h of culture, 400 μL of medium was further added in the well. NIR irradiation with a targeting temperature of 40 ºC was applied on scaffolds for 10 min every other day during the culture period. A live and dead viability kit (Molecular Probes, USA) was used to investigate the cell viability after 3 days of culture. For alkaline phosphatase (ALP) staining, the extract of different scaffolds was supplemented into the osteogenic media for cell culture. After 7 and 14 days of culture, rBMSCs were stained with ALP solution and observed using an optical microscope.

In vivo implantation of scaffolds and micro-CT analysis: All the animal surgical procedures were approved by the Animal Research Committee of Dongguan University of Technology. Twenty male Sprague-Dawley rats (10 weeks old, body weight: 300-350 g) were used for experiments. The rats were anesthetized by intraperitoneal injection of pentobarbital, then a sagittal incision of 2 cm was made on the scalp. A full-thickness defect with a dimension of 3 mm × 5 mm × 1.5 mm was made on the left side of craniums using an electric trephine drill (Nouvag AG; Goldach, Switzerland). After the creation of the cranial defects, the soft tissues were repositioned and

sutured with 4-0 silk sutures to achieve primary closure. Each rat received an intraperitoneal injection of antibiotics post-surgery. 1 week after the surgery, the rats were anesthetized again by intraperitoneal injection of pentobarbital, then a sagittal incision of 5 mm was made on the scalp. Afterward, four types of scaffolds (n = 4 for each group) with a dimension of 3.3 mm × 5.5 mm × 1 mm, were compressed and implanted into left cranial defects through a minimally invasive way with the assistance of NIR irradiation and surgical tools. Sham surgery was also conducted, in which left cranial defects were produced but no scaffolds were implanted. The soft tissues were repositioned and sutured with 4-0 silk sutures to achieve primary closure. Each rat received an intraperitoneal injection of antibiotics post-surgery. The implanted scaffolds were subjected to 10 min of NIR irradiation every other day, up to 30 days, with a target temperature of 40 ºC. After 3 months post-surgery, 20 rats were sacrificed, and obtained calvarias were scanned using micro-CT (Skyscan1176, Kontich, Belgium). The scanning was performed at a resolution of 18 μm and the images were acquired to reconstruct tomograms with 3D Creator software. The ratio of bone volume/tissue volume (BV/TV), bone mineral density (BMD) and total porosity were measured using CTAn image analysis software based on the micro-CT images. H&E staining and Masson's Trichrome staining were conducted after the sectioning of in vivo specimens embedded in paraffin to investigate histochemistry of regenerated bone tissues.

Statistical analysis: Quantitative data are expressed as mean ± s.d. 0.05 was selected as the significance level, and the data were indicated with (*) for probability less than 0.05 ($p < 0.05$).

Acknowledgments

C. Wang, H. Yue, and J. Liu contributed equally to this work. This work was supported by Dongguan University of Technology (KCYCXPT201603, TDYB2019003), Department of Education of Guangdong Province, China (2016KQNCX168), Natural Science Foundation of

Guangdong Province, China (2018A0303130019). J. Liu and Y. Tang were supported by Guangxi Science and Technology Program, China (2018GXNSFAA294116), Guangxi Science and Technology Program, China (2018GXNSFAA138074) and Scientific Research Project of High-level talents in the affiliated Hospital of Youjiang Medical College for Nationalities, China (R20196306).

Conflicts of interest

There are no conflicts of interest to declare.

Author contributions

C. Wang conceived the project. C. Wang, Z. He and K. Li conducted the scaffold fabrication, characterization, *in vitro* release/degradation test and *in vitro* cell culture. H. Yue, J. Liu and Y. Tang conducted the *in vivo* experiments in rat cranial defects and analyzed the related data. C. Wang, H. Yue, Q. Zhao, B. Lu, W. Huang, Y. Wei, Y. Tang and M. Wang contributed to the writing and revision of the manuscript.

Reference

[1] H. Ma, J. Luo, Z. Sun, L. Xia, M. Shi, M. Liu, J. Chang, C. Wu, 3D printing of biomaterials with mussel-inspired nanostructures for tumor therapy and tissue regeneration, Biomaterials 111 (2016) 138-148.

[2] A.T. Neffe, B.F. Pierce, G. Tronci, N. Ma, E. Pittermann, T. Gebauer, O. Frank, M. Schossig, X. Xu, B.M. Willie, One step creation of multifunctional 3D architectured hydrogels inducing bone regeneration, Adv. Mater. 27(10) (2015) 1738-1744.

[3] J.G. Hardy, M. Palma, S.J. Wind, M.J. Biggs, Responsive Biomaterials: Advances in Materials Based on Shape‐Memory Polymers, Adv. Mater. 28(27) (2016) 5717-5724.

[4] G. Lewis, Alternative acrylic bone cement formulations for cemented arthroplasties: present status, key issues, and future prospects, J. Biomed. Mater. Res. B Appl. Biomater. 84(2) (2008) 301-319.

[5] C. Wang, Q. Zhao, M. Wang, Cryogenic 3D printing for producing hierarchical porous and rhBMP-2-loaded Ca-P/PLLA nanocomposite scaffolds for bone tissue engineering, Biofabrication 9(2) (2017) 025031.

[6] M.A. Velasco, C.A. Narváez-Tovar, D.A. Garzón-Alvarado, Design, materials, and mechanobiology of biodegradable scaffolds for bone tissue engineering, Biomed Res. Int. 2015 (2015).

[7] Y.-J. Wang, U.-S. Jeng, S.-h. Hsu, Biodegradable water-based polyurethane shape memory elastomers for bone tissue engineering, ACS Biomater. Sci. Eng. 4(4) (2018) 1397-1406.

[8] D. Zhang, O.J. George, K.M. Petersen, A.C. Jimenez-Vergara, M.S. Hahn, M.A. Grunlan, A bioactive "self-fitting" shape memory polymer scaffold with potential to treat cranio-maxillo facial bone defects, Acta Biomater. 10(11) (2014) 4597-4605.

[9] L. Wang, Y. Qiu, H. Lv, Y. Si, L. Liu, Q. Zhang, J. Cao, J. Yu, X. Li, B. Ding, 3D Superelastic Scaffolds Constructed from Flexible Inorganic Nanofibers with Self‐Fitting Capability and Tailorable Gradient for Bone Regeneration, Adv. Funct. Mater. (2019) 1901407.

[10] R.A. Perez, J.-E. Won, J.C. Knowles, H.-W. Kim, Naturally and synthetic smart composite biomaterials for tissue regeneration, Adv. Drug Deliv. Rev. 65(4) (2013) 471-496.

[11] J.F. Mano, Stimuli - responsive polymeric systems for biomedical applications, Adv. Eng. Mater. 10(6) (2008) 515-527.

[12] W. Tao, X. Zhu, X. Yu, X. Zeng, Q. Xiao, X. Zhang, X. Ji, X. Wang, J. Shi, H. Zhang, Black phosphorus nanosheets as a robust delivery platform for cancer theranostics, Adv. Mater. 29(1)

(2017) 1603276.

[13] B. Yang, J. Yin, Y. Chen, S. Pan, H. Yao, Y. Gao, J. Shi, 2D‐Black‐Phosphorus‐Reinforced 3D‐Printed Scaffolds: A Stepwise Countermeasure for Osteosarcoma, Adv. Mater. 30(10) (2018) 1705611.

[14] C. Liu, W. Yao, M. Tian, J. Wei, Q. Song, W. Qiao, Mussel-inspired degradable antibacterial polydopamine/silica nanoparticle for rapid hemostasis, Biomaterials, 179 (2018) 83-95

[15] Q. Zhao, J. Wang, H. Cui, H. Chen, Y. Wang, X. Du, Programmed shape‐morphing scaffolds enabling facile 3D endothelialization, Adv. Funct. Mater. 28(29) (2018) 1801027.

[16] K. Hearon, P. Singhal, J. Horn, W. Small IV, C. Olsovsky, K.C. Maitland, T.S. Wilson, D.J. Maitland, Porous shape-memory polymers, Polym. Rev. 53(1) (2013) 41-75.

[17] G. Liu, Y. Zhao, G. Wu, J. Lu, Origami and 4D printing of elastomer-derived ceramic structures, Sci. Adv. 4(8) (2018) eaat0641.

[18] Y.-C. Li, Y.S. Zhang, A. Akpek, S.R. Shin, A. Khademhosseini, 4D bioprinting: the next-generation technology for biofabrication enabled by stimuli-responsive materials, Biofabrication 9(1) (2016) 012001.

[19] J. Lee, H.-C. Kim, J.-W. Choi, I.H. Lee, A review on 3D printed smart devices for 4D printing, Int. J. Precis. Eng. Manuf. - Green Technol. 4(3) (2017) 373-383.

[20] C.Wang, H. Shen, Y. Tian, Y. Xie, A. Li, L. Ji, Z. Niu, D. Wu, D. Qiu, Bioactive nanoparticle–gelatin composite scaffold with mechanical performance comparable to cancellous bones. ACS Appl Mater Interf. 6 (15) (2014) 13061-13068.

[21] C.L. Sadowsky, J.W. McDonald, Activity‐based restorative therapies: Concepts and applications in spinal cord injury‐related neurorehabilitation, Dev. Disabil. Res. Rev. 15(2) (2009) 112-116.

[22] W.A. El-Kheir, H. Gabr, M.R. Awad, O. Ghannam, Y. Barakat, H.A. Farghali, Z.M.E. Maadawi, I. Ewes, H.E. Sabaawy, Autologous bone marrow-derived cell therapy combined with physical therapy induces functional improvement in chronic spinal cord injury patients, Cell Transplant. 23(6) (2014) 729-745.

[23] T.M. Filion, J. Xu, M.L. Prasad, J. Song, In vivo tissue responses to thermal-responsive shape memory polymer nanocomposites, Biomaterials 32(4) (2011) 985-991.

[24] Z. Deng, Y. Guo, P.X. Ma, B. Guo, Rapid thermal responsive conductive hybrid cryogels with shape memory properties, photothermal properties and pressure dependent conductivity, J. Colloid Interface Sci. 526 (2018) 281-294.

[25] D. Gan, M. Liu, T. Xu, K. Wang, H. Tan, X. Lu, Chitosan/biphasic calcium phosphate scaffolds functionalized with BMP‐2‐encapsulated nanoparticles and RGD for bone regeneration, J. Biomed. Mater. Res. A 106(10) (2018) 2613-2624.

[26] Q. Cao, Z. He, W.Q. Sun, G. Fan, J. Zhao, N. Bao, T. Ye, Improvement of calcium phosphate scaffold osteogenesis in vitro via combination of glutamate-modified BMP-2 peptides, Mater. Sci. Eng. C 96 (2019) 412-418.

[27] W. Habraken, J. Wolke, A. Mikos, J. Jansen, PLGA microsphere/calcium phosphate cement composites for tissue engineering: in vitro release and degradation characteristics, J. Biomater. Sci. Polym. Ed. 19(9) (2008) 1171-1188.

[28] L. Du, S. Yang, W. Li, H. Li, S. Feng, R. Zeng, B. Yu, L. Xiao, H.-Y. Nie, M. Tu, Scaffold composed of porous vancomycin-loaded poly (lactide-co-glycolide) microspheres: A controlled-release drug delivery system with shape-memory effect, Mater. Sci. Eng. C 78 (2017) 1172-1178.

[29] L. Chen, J.X. Wang, C.Y. Tang, W.C. Law, Shape memory effect of thermal-responsive nano-hydroxyapatite reinforced poly-dl-lactide composites with porous structure, Compos. B Eng. 107

(2016) 67-74.

[30] L. Tong, Q. Liao, Y. Zhao, H. Huang, A. Gao, W. Zhang, X. Gao, W. Wei, M. Guan, P.K. Chu, Near-infrared light control of bone regeneration with biodegradable photothermal osteoimplant, Biomaterials 193 (2019) 1-11.

[31] X. Wang, J. Shao, M.A. El Raouf, H. Xie, H. Huang, H. Wang, P.K. Chu, X.-F. Yu, Y. Yang, A.M. AbdEl-Aal, Near-infrared light-triggered drug delivery system based on black phosphorus for in vivo bone regeneration, Biomaterials 179 (2018) 164-174.